The Influence of Viscosity Ratio on Mixing Effectiveness in a Two-fluid Laminar Motionless Mixer

Amy L. Ventresca, Qing Cao and Ajay K. Prasad*

Department of Mechanical Engineering, University of Delaware, Newark, DE, USA

An investigation of dependence of laminar mixing efficiency of a motionless mixer upon viscosity ratio at low Reynolds number (≤3) was performed. Viscosity ratios up to 340 were investigated. The liquids were aqueous solutions of carboxymethylcellulose (CMC). Two transparent liquid streams, one marked with a fluorescing dye, were injected into a pipe housing five elements of an SMX mixer. The degree of mixing was evaluated by imaging a downstream cross-section of pipe using laser induced fluorescence (LIF). Highly resolved spatial variations of fluorescence intensity were recorded using a CCD camera. Mathematical evaluations using correlograms, scale of segregation, COV, and intensity histograms are presented.

On a mené une étude sur la dépendance de l'efficacité du mélange laminaire dans un mélangeur statique par rapport au rapport de viscosité à un faible nombre de Reynolds (″ 3). Des rapports de viscosité allant jusqu'à 340 ont été étudiés. Les liquides étaient des solutions aqueuses de carboxyméthylcellulose (CMC). Deux courants liquides transparents, l'un marqué par un colorant fluorescent, ont été injectés dans une conduite comprenant cinq éléments d'un mélangeur SMX. Le degré de mélange a été évalué par imagerie LIF d'une section transversale aval de la conduite. Des variations spatiales hautement résolues d'intensité de la fluorescence ont été enregistrées au moyen d'une caméra CCD. Des évaluations mathématiques utilisant des corrélogrammes, une échelle de ségrégation, le coefficient de variation (COV) et des histogrammes d'intensité sont présentées.

Keywords: static mixer, SMX, viscosity ratio, laser induced fluorescence, correlogram.

Static mixers, also known as motionless or in-line mixers, constitute a low-cost option for mixing in the chemical process industry. Static mixers offer attractive features such as closed-loop operation and no moving parts, in contrast to continuously-stirred tank reactors (for example, Streiff and Rogers, 1994). The static mixer is a collection of blades which fits inside a pipe carrying the fluids to be blended. The two liquids to be mixed (typically a polymer melt and an additive) are forced through the mixer under high pressure, and they are cut and folded repeatedly as they negotiate the bends and openings within the mixer. The scale of segregation between the liquids is greatly reduced by this process such that eventually diffusion can complete the mixing process. The reduction in the scale of segregation is dependent on the liquid properties and the number and type of mixing elements. Our goal at present has been to investigate the effectiveness of static mixing in an SMX mixer between two miscible liquid streams as a function of viscosity ratio (m) and Reynolds number (Re) in the laminar flow regime.

The current study concerns the mixing of viscous fluids in the SMX geometry motionless mixer (Figure 1). The SMX is a common industrial mixer with many advantages. Numerical simulations for six common static mixer types indicate the superior overall performance of the SMX mixer (Rauline et al., 1998) and the greater efficiency of the SMX as compared to the Kenics (twisted-tape) mixer (Rauline et al., 2000). Experimental comparisons of several common motionless mixers gave the SMX high rankings for 2 out of 3 mixing criteria (Heywood et al., 1984). Its popularity and efficiency make the SMX an ideal target for further investigation.

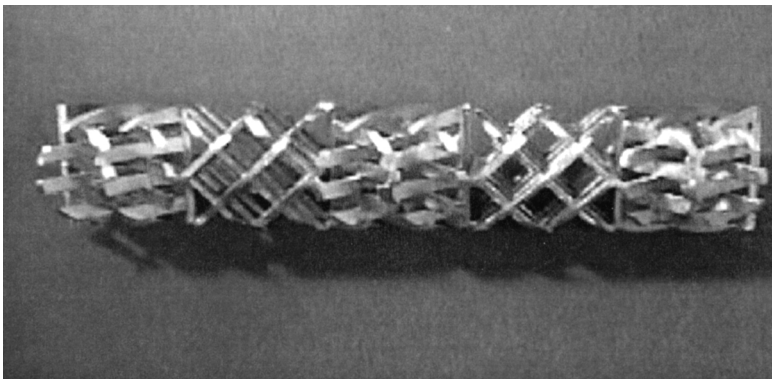

Figure 1. Close-up of a five-element Koch static mixer.

Nevertheless, experimental investigations of SMX mixer performance are limited. Schneider (1981) cites

*Author to whom correspondence may be addressed. E-mail address: prasad@me.udel.edu

the following experimentally derived equation for calculation of the necessary mixer length for high/low viscosity fluid mixing: $(L/D)_{hi/lo} = (L/D)_{hi/hi} + a \log m$, where $a = 1$ for the SMX mixer, m = viscosity ratio (high over low), D is the mixer diameter, and L is the total length of the mixer with multiple elements. This relationship indicates that high/low viscosity mixtures are less well mixed after a given number of elements than high/high mixtures. Li et al. (1997) have estimated the pressure drop, for both Newtonian and non-Newtonian fluids, across the SMX mixer, for a large range of Reynolds numbers. Fleischli et al. (1997) studied the in-situ progression of layer development and particle distribution in an SMX mixer using hardened epoxy cross-cuts, and obtained very good numerical agreement with actual particle distributions.

In contrast to the SMX mixer, the Kenics (twisted-tape) mixer appears to have received the most attention, possibly due to its greater North American popularity (Jaffer and Wood, 1998) and simpler geometry. Many experimental methods used with the Kenics are relevant to the study of the SMX. Šir and Lecjaks (1982) experimentally determined the number of Kenics mixer elements for complete homogenization of two liquids of differing viscosities (glycerol and tap water) via iodometric decolorization. Jaffer and Wood (1998) studied Kenics KM mixer elements with various L/D ratios. LIF and image analysis were used to quantify laminar mixing by measuring the average striation thickness, variance of striation widths, and interfacial area. Karoui et al. (1998) applied LIF to measure local concentrations at the outlet of different configurations of Sulzer SMV static mixers placed in a tube. They used miscible fluids (water with Rhodamine dye) and operated in the turbulent regime. Their results showed that the velocity ratio between the two streams influences the radial mixing.

Numerical techniques represent an increasingly powerful tool to study mixing in motionless mixers. Mickaily-Huber et al. (1996) found that pressure drop increases linearly with flow velocity for Sulzer SMRX static mixers, and that for a given flow velocity, the pressure drop increases with the internal mixer tube crossing angles. Mixing efficiency also depends strongly on the internal tube crossing angle; a 90 degree angle was found to be optimal. They also studied the mixing performance improvement afforded by using two elements. Numerical techniques developed by the group at the Technical University of Eindhoven (Anderson, 1999, and Kruijt, 2000) have advanced the computational study of distributive, laminar mixing. Hobbs and Muzzio (1998) investigated laminar Kenics mixer performance for a large range of Reynolds numbers. Unger and Muzzio (1999) demonstrated the effectiveness of LIF and statistical analysis for quantification of industrial mixing. Fourcade et al. (2001) applied a particle tracking method to the CFD flow field and calculated the average value for the rate of striation thinning for the SMX and Kenics mixers. Fourcade et al. (2001) also performed LIF measurements using Rhodamine WT to characterize mixing of centrally injected aqueous glucose solutions (0.8-2.2 Pa·s). Flow rates ranged from 300 to 1500 mL/min, while flow rate ratios ranged from 100 to 10 000. Bulk fluid to added fluid viscosity ratios were 1:1 and 1:8. They obtained good agreement between CFD results and LIF measurements of striation. Mean rate of striation thinning for an SMX element was found to be approximately six times higher than for a Kenics element. Whereas Fourcade et al.'s (2001) approach has been to use experimental LIF results to both confirm CFD model results for a like geometry and to compare mixtures using the rate of striation thinning, our goal in this paper is to characterize degree of mixing using various statistical measures, specifically for industrial pipe mixing. In particular, we seek to develop statistical measures which are independent of mixer geometry and fluid properties that will quantify pipe mixtures of relevance to industry.

Experimental Design

The cylindrical Koch SMX laminar pipe flow mixer (Figure 1) used in these experiments consisted of five mixing elements. Each element contained stacks of criss-crossed layers of mixing blades. Successive mixer elements having a L/D ratio of 1 and diameter of 25.4 mm are rotated by 90 degrees axially and joined.

The mixer housing, composed entirely of transparent Plexiglas, consisted of an outer rectangular box and a 25.4 mm diameter pipe into which the mixer was placed. The box was filled with mineral oil to minimize refraction, permitting undistorted axial viewing (i.e., longitudinal sections containing the axis of the cylinder). Additionally, the housing incorporated a novel downstream window which allowed 'head-on' access for undistorted viewing along transverse sections (i.e., sections perpendicular to the axis). Figure 2 is a schematic of our static mixer experimental set-up depicting the transverse recording arrangement.

Fluids were driven through the mixer by twin gear pumps (Zenith BPB-4391), with a motor range of 10-70 rpm and a displacement of 3.0 mL per revolution. The two liquids to be mixed were introduced into the static mixer tube using a T-junction as shown. The liquids were separated by a splitter plate until they entered the mixing elements. One of them, Liquid A, had a small amount of fluorescing dye homogeneously mixed with it, while the other was transparent. Upon emerging from the mixer, the two liquids had undergone a degree of mixing. Transverse cross-sections (perpendicular to the tube axis) were illuminated with frequency-doubled Nd:YAG 532 nm laser light (Continuum Surelite II, with a pulse duration of 6 nanoseconds) formed into a 1 mm thick sheet, and the resulting fluorescence was captured on a high-resolution Kodak ES 1.0 CCD camera (1k × 1k pixels). The intensity of fluorescence was proportional to the local dye concentration, and therefore to the local concentration of Liquid A. This technique, called laser induced fluorescence (LIF), was extremely effective in distinguishing Liquids A and B and could therefore be used to gauge the degree of mixing.

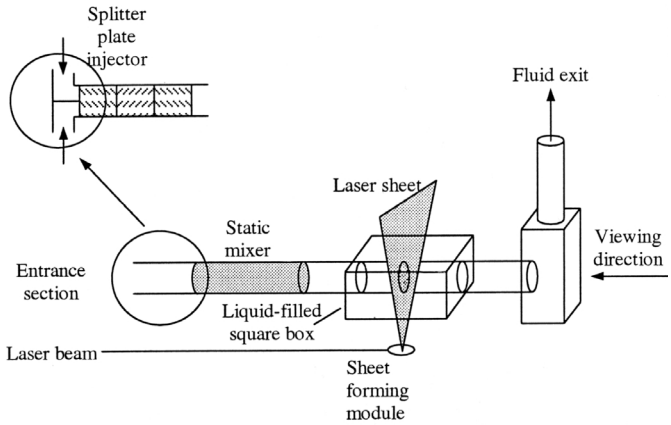

Figure 2. Schematic of experimental set-up. Laser illumination and recording arrangement is depicted for a transverse section.

The liquids were aqueous solutions of carboxymethylcellulose (CMC). The addition of even small quantities of CMC can greatly increase solution viscosity, with the solutions displaying slight shear-thinning behavior. Viscosities were varied by varying the mass percentage of CMC added. The two liquid streams were carefully density-matched by adding sugar to the stream containing the smaller amount of CMC (i.e., the lower viscosity stream). Fluid refractive indices were not substantially different from that of water, possibly because fluids contained only about 1% CMC and/or sugar by weight. Moreover, since fluid pairs were density-matched with table sugar their refractive indices were not appreciably different. Reference viscosity curves for aqueous CMC solutions with various percentages of Hercules Aqualon 7H4F grade CMC at 25°C were obtained using a Rheometrics dynamic stress rheometer (model #SR-5000) (Figure 3). Reference curve data were linearly interpolated to obtain apparent viscosities at average strain rates, where for the SMX mixer, average strain rate = $64u/D$ (Streiff et al., 1999), where u = average downstream velocity. Reynolds number was calculated using pipe inner diameter, apparent viscosity at average strain rate ($64u/D$), and average fluid velocity.

Test liquids were prepared by blending CMC into water with impellers. For viscous fluids, entrapped air was evacuated from mixtures one litre at a time by placing fluid in a Pyrex Erlenmeyer flask and applying vacuum until most of the air was removed. The gear pumps used for the experiment tended to entrain air when pumping very high viscosity liquids; therefore, the upper limit on CMC mass percentage was set at 1.25%. The lower limit of 0.014% CMC was used because lower viscosities could result in pump seizure.

In the first data set, three density-matched fluids with viscosity ratios (viscosity of dyed fluid divided by viscosity of undyed fluid) $m \cong 1$ (mass percentages of CMC 0.58%, 0.47%, and 0.28%) were considered. Two-fluid combinations with varying viscosity ratios were analyzed. The second data set considers mixing of density-matched fluids with $m >> 1$ (mass percentages of CMC 1.25%, 0.014%).

Upon emerging from the static mixer section, the flow develops for some downstream distance and subsequently converges to a parabolic profile. In the first data set, we positioned the light sheet two diameters downstream from the end of the mixer in order to allow newly formed interfaces time to diffuse. However, Grenville (2001) suggested that the flow becomes fully developed by the time it transits two diameters downstream, and therefore its structure could undergo a slight distortion compared with that at the immediate exit from the mixer. Consequently, for the second data set, LIF images were acquired as close as possible to the mixer exit (to minimize reflection of laser light, the end of the mixer was painted black). As a central square was evaluated, data should be largely unaffected by boundary distortions in either case. It should be noted that for the low *Re*'s in this study, the flow development length is extremely short; therefore, some distortion due to flow development is unavoidable.

The concentration of Rhodamine 6G used in the first and second sets of experiments was 1.8×10^{-6} M and 6.1×10^{-7} M, respectively. The recorded image was stored as an 8-bit, 1k × 1k matrix. Pictures were analyzed using in-house software (MATLAB). A central square from the cross-sectional image (side length approximately $D/2$, representing a 161 mm^2 area) was analyzed using a custom MATLAB program. The correlogram of the image was computed using fast-Fourier transforms (FFTs). (Refer to Danckwerts, 1952, for a complete discussion of the definition and measurement of the correlogram. *R(r)*, the ordinate of the correlogram, is the dimensionless correlation value for pixel pairs separated by a distance of r pixels. $-1 \leq R(r) \leq 1$.) Zero padding was used to eliminate wraparound error. Results were consistent with Harnby et al. (1992).

The software calculated individual and averaged correlograms, histograms, normalized COV (standard deviation divided by mean, normalized by unmixed COV value), and scale of segregation. A sufficient number of frames were averaged to obtain reliable statistics. Pixel distance, *r*, and modified scale of segregation, *S*, have been non-dimensionalized by an approximate striation width, *d*. While somewhat arbitrary, this value was chosen based on the averaged striation width values for 0.58%/0.58% CMC over all pump speeds. The consistent structure of this particular fluid combination's resulting images was regarded

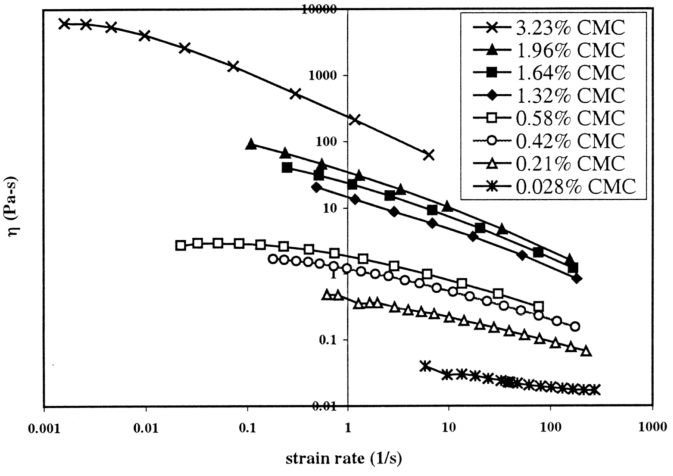

Figure 3. Viscosity of aqueous CMC solutions with various percentages (by mass, sugar mass not included) of Hercules Aqualon 7H4F CMC (25°C) as a function of strain rate. (Margin of error +/–2%.)

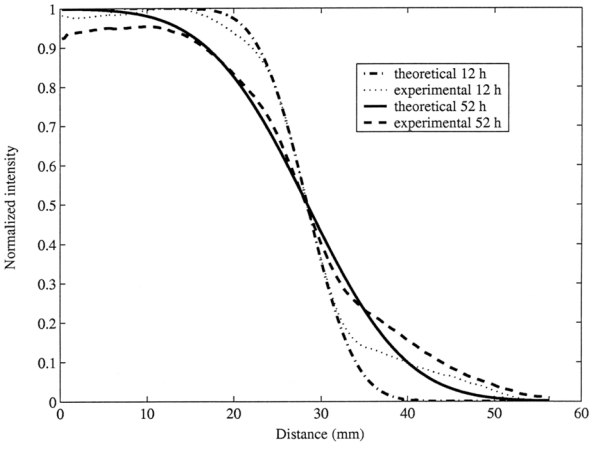

Figure 4. Diffusion of Rhodamine 6G from 1.25% CMC solution (6.1×10^{-7} M) to undyed 0.014% CMC solution. $D \approx 2 \times 10^{-10}$ m^2/s. Profiles at only two times are shown for clarity. Least squares fit is performed over a restricted neighborhood of the interface.

Figure 5. Cross-sections of blending dyed and undyed 0.58% CMC solution (m=1). From left to right, 60, 240, and 420 mL/min (10, 40, and 70 rpm pump speeds, respectively). As expected, structures with sharpest contrast occur at the lowest residence time, while diffusion produces rounder, more diffuse images.

Figure 6. Cross-sections of 1.25% CMC solution (light colored fluid) blending with 0.014% CMC solution. From left to right, 60, 240, and 420 mL/min (m=340, 257, and 201, respectively). Note the decrease in structural size with increasing flow rate and the 'clumpy' structural appearance.

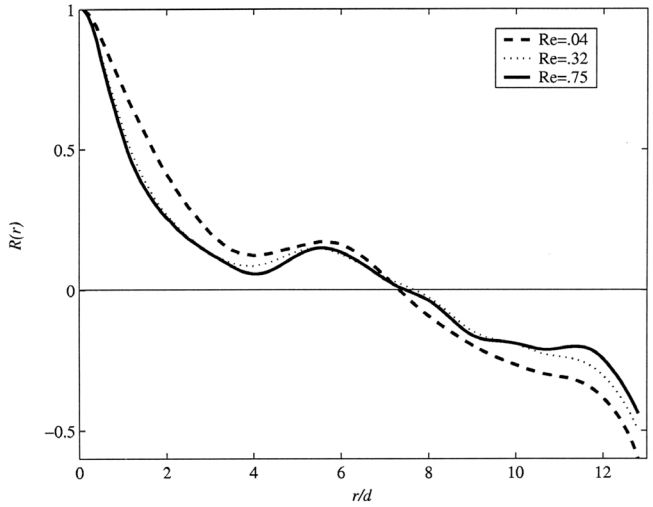

Figure 7. Variation of correlogram with Re for 0.58% CMC solution (m = 1, d = 40 pixels = 1 mm).

to be especially characteristic of the SMX geometry. The value of d was approximately 40 pixels, corresponding to about 1.0 mm in the physical plane. Of course, it varied somewhat from case to case, but as will be seen subsequently, $d \approx 40$ pixels fell in the middle of the range of variation and is therefore a suitable value.

It has been suggested (Etchells, 2001) that the use of Rhodamine dye to evaluate mixing beween two liquid streams might be misleading, because the dye might diffuse from the dyed stream to the clear stream at a rate exceeding the diffusion of CMC molecules. Unfortunately, the literature does not contain data regarding the diffusion of Rhodamine from a viscous CMC solution into a less viscous one. We therefore performed an experiment to measure the diffusion coefficient of Rhodamine 6G as follows. A layer of dyed (6.1×10^{-7} M) 1.25% CMC fluid was placed in a small rectangular Plexiglas tank. Using a stopcock, slow, careful addition of undyed 0.014% CMC fluid above the dyed fluid resulted in two horizontal layers of fluid. Every 10 h, the tank was illuminated with a sheet of light, and a digital image of fluorescence intensity was acquired. A long-wavelength filter was used to eliminate elastic scattering from the Nd:YAG laser. For each image, the vertical intensity distribution was averaged over ten central columns. Next, an analytical solution was obtained for the intensity profile. The analytical solution was matched to the experimental data using a least-squares approach to obtain a diffusion coefficient of 2×10^{-10} m^2/s (Figure 4). It should be remembered that the diffusion coefficient could vary for other combinations of viscosity. This value of diffusivity is similar to that measured by Hansen et al. (1998) for diffusivity of Rhodamine 6G in water/methanol solutions, implying that the presence of CMC does not significantly impede the mobility of dye molecules. The Stokes-Einstein equation indicates that the CMC molecules will themselves diffuse much more slowly owing to their larger molecular weight. Consequently, the discussion pertaining to diffusion in the forthcoming section must be interpreted with care, i.e., the discussion refers to the diffusion of dye, and not to the CMC molecules. Despite this shortcoming, comparative conclusions are possible for the different mixing effectiveness measures examined in this study.

Results

Qualitative Observations: Mixture Cross-Sections

Figure 5 shows representative low m cross-sections at three different pump speeds. For low m data sets, the sharpest image with the largest contrast and most elongated structures appears at the highest pump speed, while the lowest pump speed image shows diffuse, rounded structures. In the high m images (Figure 6), however, the fluid is not drawn into elongated structures; instead dark and light fluid exhibit more rounded cross-sectional features. Even when these forms are broken up into small pieces, intensity differences are preserved. An additional difference of the high m images with their low m counterparts is that the mixture quality demonstrates a greater dependence upon pumping speed at high m, demonstrating a dramatic reduction in structure size as flow rate is increased. The most elongated structures can be seen for m = 340; these are much more 'broken up' for higher pump speeds. Diffusion is likely to bear the most influence at higher pump speeds, since interfacial surface area is so much greater. Conversely, in low m cases, structure appears to be preserved despite increasing pump speed, so that diffusion bears the most influence at the lowest pump speed.

Statistical Analysis (Low m)

Correlograms

Figure 7 shows three correlograms (at 60 mL/min, 240 mL/min, and 420 mL/min) for the mixing of two 0.58% CMC solutions (these correlograms correspond to the images shown in Figure 5). Images were acquired approximately 2D downstream of the mixer. Some correlogram features for low m seem to be characteristic of

our SMX mixer and input geometry, including a slope tending to zero as *r* tends to zero, an elongated 'tail' before the correlogram drops to zero, a small peak at 240 pixels (6 mm in the physical plane), and negative (but smaller) values at large distances. The slopes of the curves drop to zero as *r/d* tends toward zero, indicating the two fluids are miscible and undergoing diffusion. 'Tails' are characteristic of the elongated fluid shapes displayed in our pictures. A small peak at about 240 pixels ($r/d = 6$) appears to be indicative of underlying mixture structure. The correlation becomes negative at $r/d \sim 8$, indicating that large scale structure persists despite passage through five mixer elements. The value of *r/d* at which the correlogram undergoes a zero-crossing is proportional to the spatial separation between light and dark blobs in the LIF image. In Figure 7 this corresponds to $r/d = 8$ or about 8 mm in the physical image. As expected, all three curves undergo a zero crossing at the same value of *r/d*. This is because, for low *m*, the larger structures are identical and independent of flow rate, although the small scale structures show the effects of diffusion (diffusion is a more significant effect for small-scale structures due to larger relative interfacial area). The relative elongation of the correlogram is less for slower pump speeds, reflecting the more rounded structure shape.

Modified Scale of Segregation

Danckwerts (1952) has suggested the scale of segregation, the area under the positive correlogram, as an indication of structure radius. The scale of segregation did not enable an accurate relative comparison of some correlograms which dipped to zero before the small peak and tail, then returned to positive values, so that the statistic was understated for these cases. To enable relative comparisons, a modified scale of segregation statistic was calculated using four times the triangular area beneath the correlogram and above the $R(r) = 0.5$ line. This measure is obtained by linearly extrapolating the correlogram for $1.0 \geq R \geq 0.5$ to $R = 0$. The *S/d* values for 0.58%/0.58% CMC at 60, 240, and 420 mL/min (10, 40, and 70 rpm, respectively) are 1.59, 1.06, and 0.98, respectively, indicating that the structure exhibits smaller length scales at higher flow velocities, because the reduced residence time at higher velocities is inadequate to enable diffusional smoothing at small scales. These trends are seen consistently across the entire low *m* set of experiments. As shown in Figure 8, *S/d* drops sharply with *Re* for $Re < 0.5$, then flattens out for higher *Re*. For miscible fluids, therefore, scale of segregation as a measure of mixing effectiveness must be interpreted with care. Scale of segregation may not constitute an adequate indicator of degree of mixing, since improved mixture quality evidences large, homogeneously blended structures and consequently larger values of structure radius.

Intensity Histograms

Figure 9 shows the intensity histograms corresponding to the images in Figure 5. Histogram standard deviation for 60, 240, and 420 mL/min (10, 40, and 70 rpm, respectively) is 14.7, 15.7, and 17.1, respectively. This result corroborates the correlation results earlier, and indicates that the lower speed histogram is more uniform in dye concentration and produces a narrower histogram (smaller contrast). The mean value of the intensity distribution tends to increase with pump speed, possibly indicating that intensity response could be slightly nonlinear with concentration. Histograms appear symmetric about the mean (small skewness). The lack of bimodality in the intensity distributions was unexpected and can be attributed to several factors. It is possible that internal reflectance of fluorescence and the blurriness that results from imaging through a substantial depth of dye-laden liquid can artificially reduce the contrast and lead to a suppression of the bimodal distribution. However, the two liquids in our system are completely miscible and therefore Rhodamine, being soluble in both fluids, is unhindered in its diffusion across fluid phases (as confirmed by our diffusion measurements). In fact, LIF images reveal that the gray color is not uniformly distributed, but is consistently located along the interface between fluids. This suggests that the peak of the histogram may be in fact correctly situated at an intermediate intensity.

Normalized COV

COV values were normalized with an initial COV_0 value, referring to intensity standard deviation divided by mean intensity for the unmixed fluid at the injection stage. Ideally, the COV_0 value should approach 1.0; due to background noise, however, this value must be computed on a case-by-case basis.

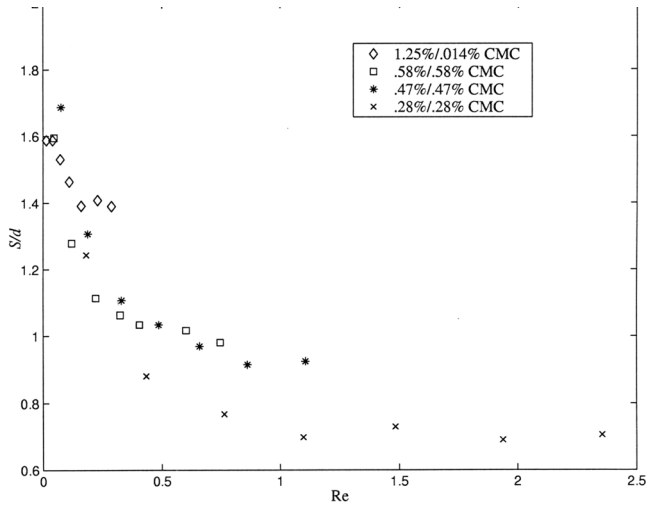

Figure 8. Variation of modified *S/d* with *Re* (*d* = 40 pixels = 1 mm).

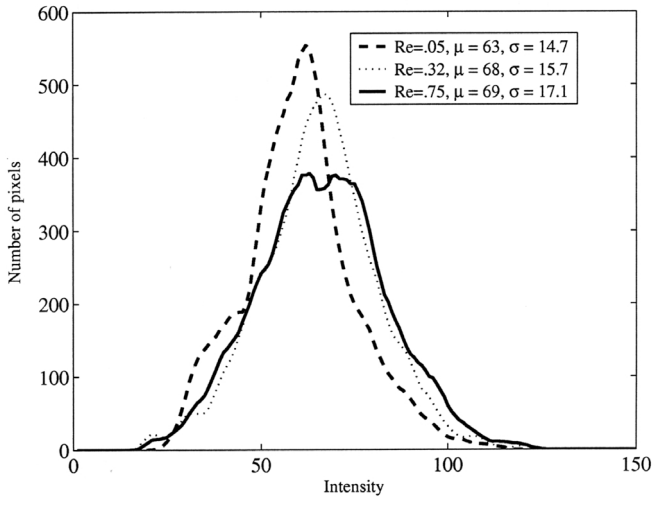

Figure 9. Variation of intensity histogram with *Re* for 0.58% CMC fluid (*m* = 1).

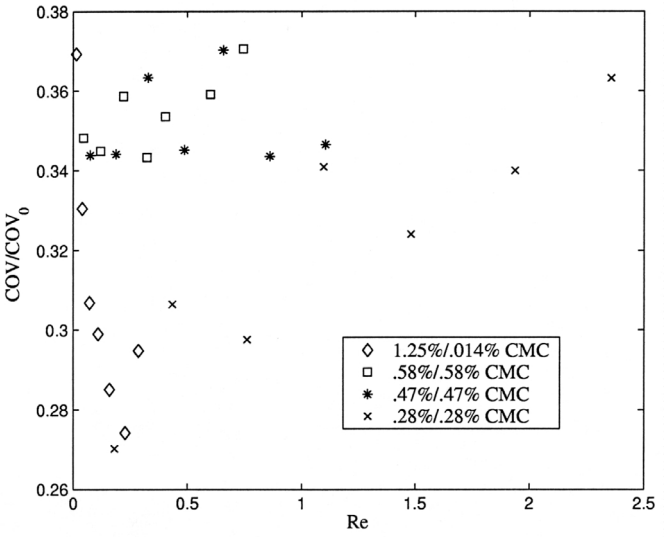

Figure 10. Variation in normalized COV with *Re* for high and low *m* values.

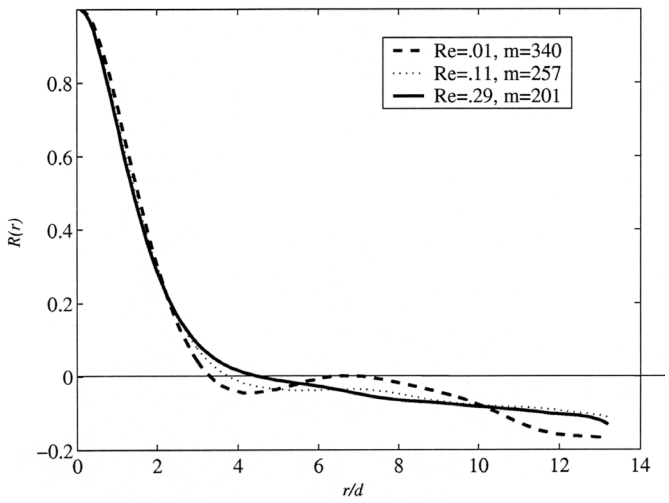

Figure 11. Variation in correlogram for a combination of 1.25% CMC solution and 0.014% CMC solution.

Normalized COV values for 60, 240, and 420 mL/min (10, 40 and 70 rpm, respectively) for 0.58%/0.58% solution were 0.35, 0.34, and 0.37, respectively. This statistic is lowest for the 240 mL/min (40 rpm) data set, indicating the best mixture, contrary to other indicators. One reason the 240 and 420 mL/min normalized COV values could be lower than expected is due to the upward shift in the mean intensity value for these two data sets. Because intensity range and mean intensity can differ for different fluid combinations, comparisons within the data set are most informative. Variation in COV, although small, appears to be significant. Two of the three low *m* mixtures evaluated displayed an increasing trend in normalized COV with *Re* (Figure 10), while the third data set appeared to have a somewhat constant normalized COV value for all *Re* values.

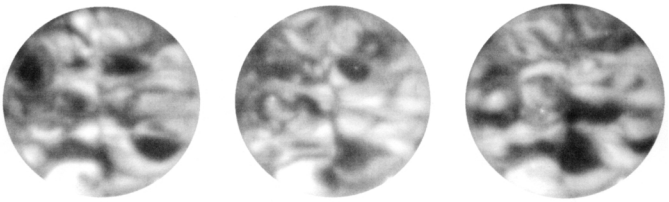

Figure 12. Three images picked at random from a set of 55 sequential images show the amount of temporal variation in cross-sectional structures encountered at high *m* (here *m* = 340). Dark and light blobs of fluid tend to move in inconsistent ways. For example, the rightmost image has a large patch of dark fluid in the lower right quadrant, while the other images do not.

Statistical Analysis (High *m*)

Correlograms

High *m* correlograms drop to zero much more quickly than low *m* correlograms, indicating significantly less elongated structures (Figure 11, corresponding to the images shown in Figure 6). There is no evidence of the small peak at 240 pixels displayed by the lower *m* cross-sections. Large-scale segregation is far less important, as *R* is relatively small at large distances. Although high *m* images indicate greater differences with pumping speed, correlogram structure is much less sensitive to pump speed for large *m*. The smallest *m* value displays the longest correlogram tail, meaning the largest degree of elongation, an indication not verified by the cross-sectional pictures. Additionally, high *m* images are temporally inconsistent (Figure 12), displaying substantial frame-to-frame variations. In contrast, the low *m* images do not exhibit such variations.

Modified Scale of Segregation

Structure radius decreases with increasing pump speed (*S/d* ratios of 1.59, 1.46, and 1.39 for 60, 240, and 420 mL/min, respectively), but not appreciably, compared with *S/d* values for low *m* (Figure 8). Again diffusional effects increase the amount of homogeneously colored fluid at the small scales and hence artificially increase structure radius. For high *m*, diffusional effects are most evident at higher pump speeds. The *S/d* curve sharply decreases for $Re \leq 0.1$ then flattens out; in the low *m* curves, the sharp decline in *S/d* can still be seen for higher *Re* values.

Intensity Histograms

Intensity histograms show significant differences when compared with their low *m* counterparts (Figure 13, corresponding to images in Figure 6). First, the mean value of the intensity distribution increases with *m* (174.5, 175.2, and 178.8, for *m* = 201, 257, and 340, respectively). This indicates that the dyed fluid occupies increasingly greater portions of the cross-sectional areas as *m* increases. It has been suggested (Doraiswamy, 2001) that at high values of *m*, the phenomenon of fingering may occur, wherein the low viscosity fluid moves at a higher speed compared with the high viscosity fluid. Due to conservation of mass, the higher velocity (undyed, hence darker) fluid must occupy a smaller cross-sectional area. Such a fingering phenomenon has also been observed by Cao et al. (2000)

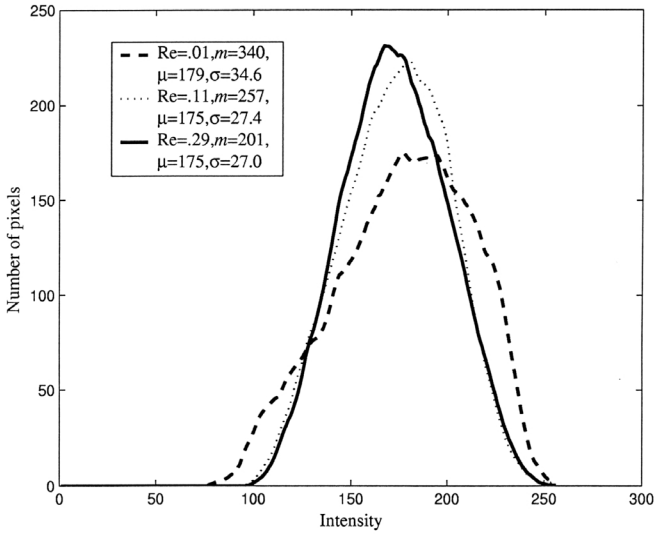

Figure 13. Variation of intensity histogram with pump speed for combination 1.25% CMC fluid and 0.014% CMC fluid.

during the centerline injection of a low-viscosity core flow into a higher viscosity coflow in a circular tube. Second, the high *m* histograms exhibit increasingly negative values of skewness as *m* increases (skewness/σ^3 values of 0.05, –0.12, and –0.30 for *m* = 201, 257, and 340, respectively). Negative skewness implies that large negative excursions of intensity from the mean value are more common than large positive excursions. It therefore appears that the low viscosity fluid might be transiting through the mixer at a higher speed and consequently undergoing reduced diffusional mixing. Such a fingering phenomenon should be visible in the longitudinal view. These experiments are planned and will be reported at a future date.

Normalized COV

Normalized COV values for 60, 240, and 420 mL/min were 0.37, 0.30, and 0.29, respectively (Figure 10). The smallest value was for 420 mL/min, indicating the best mixture. This statistic appears to decrease linearly with *Re*.

Conclusions

For low *m* data sets, statistical descriptions have served as important indicators of mixing effectiveness which reinforce our qualitative assessments of mixture cross-sections. For small *m*, the correlogram is a viable statistic for indication of goodness of mix, but can be misleading when diffusion occurs, resulting in overstatement of structural radius for low flow rate. For high *m*, temporal inconsistencies could attenuate important structural information from the correlogram, and diffusional effects diminished reduction in structural radius for high flow rate. Histograms and COV have proved to be valuable tools for both low and high *m* values. For high *m*, fingering behavior appears to be occurring and will need to be verified with longitudinal cross-sectional study.

Acknowledgements

This work was partially supported by an Educational Aid Grant from Dupont. We gratefully acknowledge the support provided by Drs. D. Massouda, A. Etchells, and R. Grenville (DuPont). The mixer housing and inlet geometry was designed by Dr. K. R. Sreenivas. The authors wish to thank B. Tande and S. Shenoy for viscosity measurements, and Hercules Aqualon for the CMC7H4F used in these experiments.

Nomenclature

COV	coefficient of variance (the standard deviation divided by the mean)
COV_0	initial coefficient of variance (COV), referring to intensity standard deviation divided by mean intensity for the unmixed fluid at the injection stage
d	average width of layers downstream from mixer, (about 40 pixels or 1 mm)
D	pipe diameter, (m)
L	length of a single mixing element, (m)
m	dimensionless viscosity ratio: viscosity of dyed fluid divided by viscosity of undyed fluid
M	concentration, (mol/L)
r	pixel distance between two points in mixture
Re	Reynolds number, calculated using pipe inner diameter, apparent viscosity at average strain rate (64*u*/*D*), and average fluid velocity
R(r)	dimensionless correlation value for pixel pairs separated by a distance of *r* pixels; –1 ″ *R* ″ 1 (refer to Danckwerts, 1952)
S	modified scale of segregation (pixels). Danckwerts (1952) has suggested the scale of segregation, the area under the positive correlogram, as an indication of structure radius. The modified scale of segregation statistic was calculated using four times the triangular area beneath the correlogram and above the *R(r)* = 0.5 line.
u	average velocity in pipe downstream from mixer, (m/s)

Greek Symbols

η	viscosity, (Pa·s)
σ	standard deviation

References

Anderson, P.D., O.S. Galaktionov, G.W.M. Peters, F.M. Van de Vosse and H.E.H. Meijer, "Analysis of Mixing in Three-Dimensional Time-Periodic Cavity Flows", J. Fluid Mech. **386**, 149–166 (1999).

Cao, Q., A. Ventresca and A.K. Prasad, "Instabilities During Centerline Injection of a Lower Viscosity Fluid into a Higher Viscosity Miscible Coflow", presented at the 53rd APS/DFD Meeting, November 19–21, 2000, Washington, DC (2000).

Danckwerts, P.V., "The Definition and Measurement of Some Characteristics of Mixtures", Appl. Sci. Res., Section A **3**, 279–296 (1952).

Doraiswamy, D., Private communication (2001).

Etchells, A., Private communication (2001).

Fleischli, M., M. Wehrli, F.A. Streiff and E. Lang, "Effect of Diffusion and Heat Conduction on Homogeneity in Laminar Static Mixing", Récents Progrès en Génie des Procédés **11**, 283–290 (1997).

Fourcade, E., R. Wadley, H.C.J. Hoefsloot, A. Green and P.D. Iedema, "CFD Calculation of Laminar Striation Thinning in Static Mixer Reactors", Chem. Eng. Sci. **56**, 6729–6741 (2001).

Grenville, R., Private communication (2001).

Hansen, R.L., X.R. Zhu and J.M. Harris, "Fluorescence Correlation Spectroscopy with Patterned Photoexcitation for Measuring Solution Diffusion Coefficients of Robust Fluorophores", Anal. Chem. **70**, 1281–1287 (1998).

Harnby, N., M.F. Edwards, and A.W. Nienow, "Mixing in the Process Industries", 2nd ed. Butterworth-Heinemann Ltd., Toronto, ON (1992).

Heywood, N.I., L.J. Viney and I.W. Stewart, "Mixing Efficiencies and Energy Requirements of Various Motionless Mixer Designs for Laminar Mixing Applications", Fluid Mixing II, I. Chem. Eng. Symp. Ser., No. **89**, 147–176 (1984).

Hobbs, D.M. and F. Muzzio, "Reynolds Number Effects on Laminar Mixing in the Kenics Static Mixer", Chem. Eng. J. **70**, 93–104 (1998).

Jaffer, S.A. and P.E. Wood, "Quantification of Laminar Mixing in the Kenics Static Mixer: An Experimental Study", Can. J. Chem. Eng. **76**, 516–521 (1998).

Karoi, A., F. Hakenholz, N. Le Sauze, J. Costes and J. Bertrand, "Determination of the Mixing Performance of Sulzer SMV Static Mixers by Laser Induced Fluorescence", Can. J. Chem. Eng. **76**, 522–526 (1998).

Kruijt, P.G.M., "Analysis and Optimization of Laminar Mixing: Design, Development and Application of the Mapping Method", Technische Universiteit Eindhoven, PhD Thesis, Eindhoven, The Netherlands (2000).

Li, H.Z., C. Fasol and L. Choplin, "Pressure Drop of Newtonian and Non-Newtonian Fluids across a Sulzer SMX Static Mixer", Trans. IChemE, Part A **75**, 792–796 (1997).

Mickaily-Huber, E.S., F. Bertrand, P. Tanguy, T. Meyer, A. Renken, F.S. Rys and M. Wehrli, "Numerical Simulations of Mixing in an SMRX Static Mixer", Chem. Eng. J. **63**, 117–126 (1996).

Rauline, D., J.-M. Le Blévec, J. Bousquet and P.A. Tanguy, "A Comparative Assessment of the Performance of the Kenics and SMX Static Mixers", Trans. IChemE, Part A, **78**, 389–395 (2000).

Rauline, D., P.A. Tanguy, J.-M. Le Blévec and J. Bousquet, "Numerical Investigation of the Performance of Several Static Mixers", Can. J. Chem. Eng. **76**, 527–535 (1998).

Šir, J. and Z. Lecjaks, "Pressure Drop and Homogenization Efficiency of a Motionless Mixer", Chem. Eng. Commun. **16**, 325–334 (1982).

Schneider, G., "Continuous Mixing of Liquids using Static Mixing Units", Reprint from PACE (1981), pp. 32–42.

Streiff, F.A., S.A. Jaffer and G. Schneider, 3rd International Symposium on Mixing in Industrial Processes", Osaka, Japan (ISMIP-3) (1999), pp. 107–114.

Streiff, F.A., and J.A. Rogers, "Don't Overlook Static-Mixer Reactors", Chem. Eng. **June**, 77–82, (1994).

Unger, D.R. and F.J. Muzzio, "Laser-Induced Fluorescence Technique for the Quantification of Mixing in Impinging Jets", AIChE J. **45** 2477–2486 (1999).

Manuscript received October 30, 2001; revised manuscript received July 22, 2002; accepted for publication July 29, 2002.